

We are IntechOpen, the world's leading publisher of Open Access books Built by scientists, for scientists

6,900

Open access books available

186,000

International authors and editors

200M

Downloads

Our authors are among the

154

Countries delivered to

TOP 1%

most cited scientists

12.2%

Contributors from top 500 universities



WEB OF SCIENCE™

Selection of our books indexed in the Book Citation Index
in Web of Science™ Core Collection (BKCI)

Interested in publishing with us?
Contact book.department@intechopen.com

Numbers displayed above are based on latest data collected.
For more information visit www.intechopen.com



Chapter

The PV/Wind System for Sustainable Development and Power Generation with Real Dynamic Input Datasets in the Distribution Power Systems

*Emel Bakmaz, Kemal Aygul, Burak Esenboga,
Tugce Demirdelen and Mehmet Tumay*

Abstract

Rapid population growth and industrialization in developing countries cause an increase in demand for energy. In order to meet this energy demand, two types of resources are used: renewable energy and nonrenewable energy. Nonrenewable sources, also called fossil fuels, cause environmental problems in serious and dangerous dimensions. For this reason, it is a necessity to find alternatives. It is a renewable energy source that can be used as an alternative to fossil fuels. This chapter deals with power control of a PV/wind system for power generation with dynamic input dataset. The main contribution of this chapter is that it is the first time to use real data from PV/wind system and observe the system reliability with real-time simulation results. The proposed system consists of doubly fed induction-based wind generator, rotor-side converter (RSC), grid-side converter (GSC), solar arrays, DC-DC converter and grid-side converter, and grid and dynamic loads. The aim of the proposed strategy is to use wind and solar energies with maximum efficiency by simulating the real condition of wind and insolation with input datasets. The modeling and the validation of the operation of the system and its controllers are done by using PSCAD/EMTDC.

Keywords: energy demand, renewable energy, PV/wind system, power generation, dynamic input, residential neighborhood

1. Introduction

Energy demand increases with industrialization, population growth, and technological development day by day, so the concept of energy has gained much attention, and sustainability of energy resources is one of the most significant issues and problems in the world today. The rapid depletion of energy resources, the unconscious use of resources such as petroleum, coal, and nuclear energy that are not self-renewing, and the pollution from these resources in the environment and

in the atmosphere have led people to use renewable energy resources. To meet the world's ever-increasing energy needs, scientists have done a lot of work to popularize the use of renewable energy sources in all areas and have developed projects like solar batteries to use the sun and projects to use windmills that make use of wind power. In this chapter, real data is obtained from solar panels and wind turbines in Adana, located in the Mediterranean region, and then used in simulation modeling and analysis. Solar and wind energy potential maps are shown for Adana in **Figure 1**.

Looking at recent studies in the literature, it seems that studies on the subject have increased in recent years. González, Riba, and Rius [1] presented a methodology for optimization of life cycle cost of hybrid renewable energy systems (HRES) based on wind, solar photovoltaic (PV), and biomass power. It is stated that HRES are alternative to enhance renewable energy production worldwide. Jain, Karampuri, and Somasekhar [2] proposed an induction motor pumping system which is fed from solar PV. They integrated the variable frequency control, sample-averaged zero-sequence elimination, and the maximum power point tracking (MPPT) algorithms in order to keep the system stable under various environmental situations. Long, Eghlimi, and Zhang [3] offered an optimization model to optimize the hourly load dispatch and the structure of a PV/wind hybrid system. They have stated that the stable operation of the hybrid power system is a more dependent wind power system than PV power system. Patra, Ray, and Mohanty [4] examined a stand-alone wind-diesel-PV hybrid system and found that the main issues are in compensating the reactive power and regulating the transient as a stable. Authors showed by simulations that transient voltage balance case in UPFC is more functional than that of STATCOM and SVC and the efficiency of UPFC with fuzzy sliding mode is enhanced compared to PI and fuzzy PI controller. Parida and

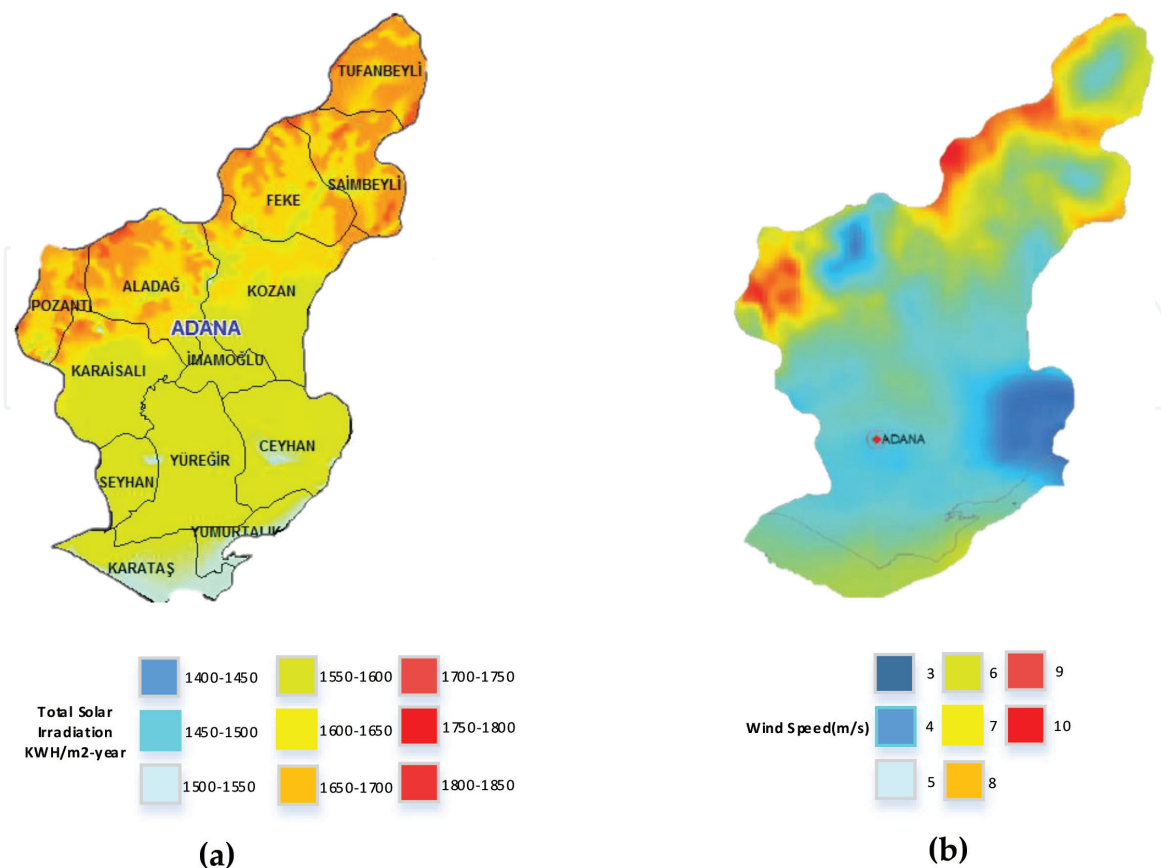


Figure 1. Adana energy potential map. (a) Adana solar energy potential map and (b) wind energy potential map.

Chatterjee [5] proposed a strategy for controlling rotor current of doubly fed induction generator (DFIG) in wind-solar hybrid system to improve generation capacity of WECS in the system. Al-Masri and Ehsani [6] performed a study about economic aspects of connecting a wind-PV hybrid system into the Jordanian power system. Shen C. and Shen Y. [7] proposed an output filter integrated to a novel dual-input photovoltaic-wind converter (DIPWC), and operation principles are summarized at this study. Solar photovoltaic power and wind turbine energy are operated at the same time and individually. 1-kW prototype power converter is built and measured to verify the correctness of the DIPWC. Also, it is mentioned that key part of the DIPWC is the inductor at the output. Cho, Chun, and Hong [8] proposed an algorithm for size optimization of a hybrid system that consists of battery, solar PV, wind generator, and diesel generator. For the performance evaluation of the proposed method, MATLAB is used. Kalla et al. [9] proposed adaptive sliding mode control algorithm for a micro-grid (MG) consisting of hydropower and wind and solar PV generation systems in order to control micro-grid voltage and frequency and also improve power quality of micro-grid.

Palmer et al. [10] studied the impact of solar radiation on the geographical distribution of solar installations. They observed that variations on irradiance may be reduced by the aggregate of the installations in the neighborhood. Ekstrom et al. [11] presented a methodology for evaluating the volatility of a system which contains both PV and wind energy generation systems. A year scale scheduling method based on interval optimization for hydro-PV-wind hybrid system is proposed by Liu, Tan, and Jiang [12]. The method is implemented on a real case study in Yunnan. Luna et al. [13] modeled and designed an energy management system and integrated it to a micro-grid. Shanthi, Uma, and Keerthana [14] proposed a power transfer scheme by minimizing the number of converters used for PV/wind system connected to the grid. Authors stated that the proposed system is capable of simplifying the process of integration of DC systems into AC system. In [15] a micro-grid which consists of renewable sources, battery, and energy management system for mentioned elements is proposed. In [16] wind-PV hybrid system which is capable to operate in on-grid and off-grid modes and developed a power management strategy for the mentioned system is proposed. Askarzadeh [17] proposed a system that integrates solar PV and wind and tidal energies with the battery storage system and proposed crow search algorithm (CSA) for the optimization of the proposed system. Kant, Jain, and Singh [18] integrated diesel-wind-PV sources with BESS as a stand-alone micro-grid. Rezkallah et al. [19] conducted a study to deal with the design process and application of active power control (APC) to reduce the number of sensors at the wind-PV-battery energy combination hybrid autonomous power generation system. Modeling, stability analysis, control design, and parameters of this hybrid combination of power generation system are presented.

Tiwari, Singh, and Goel [20] conducted a study about autonomous wind-solar hybrid energy system. Theoretical and experimental validation of autonomous wind-solar hybrid system consisting of a wind generator with doubly fed induction generator and solar PV array is also done. The new system is modeled in MATLAB and under negative conditions such as varying load, unstable wind speeds, and solar irradiation, and stator windings of DFIG are balanced with low total harmonic distortion (THD). The prototype of the system is developed using 3.7 kW DFIG and 5 kW solar array simulator to validate the simulation results. A study by Einan, Torkaman, and Pourgholi [21] conducts a new methodology or technique for isolated micro-grid including battery energy storage systems. To confirm the performance, fuzzy controller and cuckoo optimization algorithm are checked against particle swarm optimization (PSO) algorithm and genetic algorithm. The optimized fuzzy-cuckoo controller relatively differs from the other methods, and results

showed that the fuzzy-cuckoo controller has better performance than other methods.

Ji et al. [22] presented the benefits of the wind and PV combined energy storage and transmission dual power generation system. To analyze the benefits of the wind-PV combined system, a multi-angle evaluation index system of the wind/PV/energy storage is designed. Mendoza, Sumper, and Arellano [23] conducted a case study for reducing the fossil fuel consumption by generating electricity from renewable energy sources. Two systems are selected from 12 system designs. The technique used in this study can be implemented to the SIDS or other small islands in order to plan island electricity systems that will reach low emission targets in their electricity generation.

The effect of PV and variable speed wind power plants on the frequency response of the US Eastern Interconnection and Texas Interconnection is investigated by Liu, You, and Liu [24]. Controlling the frequency of the power system is also investigated. Validated system models are simulated and compared with realistic renewable information. In addition, inertia and governor control are introduced. Results show that the governor and inertia control reduced the effect of the increasing renewable penetration levels on the frequency response of the US Eastern Interconnection and Texas Interconnection and, also, show that optimal solution has higher reliability and fewer greenhouse gas emission.

The study by Hussain et al. [25] presents the optimization method named iterative filter selection approach to design the hybrid renewable energy system with maximum reliability and minimum project cost. The system includes battery storage, wind turbine, photovoltaic arrays, AC load, and dump load. As iterative filter selection approach is performed, minimization of surplus power is considered in the design process. Moreover, the proposed method is compared with some other techniques in the literature. Results show that duration analysis or computational time shortens and dump load size tolerance is shorted out for better results. Akram, Khalid, and Shafiq [26] conducted capacity optimization and development of the hybrid energy storage system resources such as wind-solar and battery-supercapacitor in a grid-connected MG. Optimization problems are formulated and solved to decrease computational time and complexity of the system. Optimization method is based on a few factors about the MG system. This method is tested using real power demand, solar irradiation, and wind speed data.

Akram, Khalid, and Shafiq [27] presented two iterative algorithms to determine appropriate sizes of renewable energy resources and energy storage for economic, reliable, and efficient operation. These algorithms named as source sizing algorithms and battery sizing algorithms are used to avoid over- and undersizing. Also, forced outage rates of wind turbine and PV and the utilization factor of battery energy storage system are considered, and the effectiveness of the proposed approach is depicted thanks to MATLAB simulation results. Gonzales et al. [28] presented a method for analyzing the stability of weak power system. It is emphasized that the main effects on weak power systems are decreasing voltage regulation and decreasing primary frequency regulation. PV power plants and wind farms proposed and validated using the real system in Bolivia due to this reason. Khaled, Eltamaly, and Beroual [29] implemented PSO to ensure the optimal power flow. Authors also introduced a study about optimal power flow of a power system integrated with distributed wind and PV as renewable distributed generation elements. The purpose of optimal power flow researches is to optimize certain objectives by adjusting power system variables. Modified PSO is used in simulation to achieve the global minimum more accurately and faster than other methods. Results show that the cost of generation and operation can be reduced by using renewable distributed generation.

This chapter presents the power control of a PV/wind system for power generation with dynamic input dataset. One of the most significant and main advantages of this chapter is that it is the first time to use real data from PV/wind system and observe the system reliability with real-time simulation results. The proposed system consists of doubly fed induction-based wind generator, rotor-side converter, grid-side converter, solar arrays, DC-DC converter, and grid and dynamic loads. The aim of the proposed strategy is to use wind and solar energy with maximum efficiency by simulating the real condition of wind and insolation with input datasets. The modeling and the validation of the operation of the system and its controllers are done by using PSCAD/EMTDC. To confirm the control, design, and the operation of the proposed system, the detailed review is done, and the simulation results are shown and indicated.

Due to the restrictions among existing literature, the aim of this chapter is as below:

1. To deal with power control of a PV/wind system for power generation
2. To use real data from PV/wind system and observe the system reliability with real-time simulation results
3. To acquire simulation results and theoretical analysis from a real industrial network model in PSCAD
4. To consist of doubly fed induction-based wind generator, RSC, GSC, solar arrays, DC-DC converter grid, and dynamic loads
5. To use wind and solar energies with maximum efficiency by simulating the real condition of wind and insolation with input datasets
6. To confirm the control system and the operation of the proposed system

This chapter primarily demonstrates the aforementioned six objectives of the proposed system.

2. Design of the proposed system

The proposed system consists of two parts: PV and wind system. These systems are examined in detail.

2.1 Solar photovoltaic system

2.1.1 Solar photovoltaic panel

The solar energy is converted into DC electrical power by a photovoltaic (PV) system. The parameters of an equivalent circuit of a PV are the open-circuit voltage (V_{oc}), the short-circuit current (I_{sc}), the maximum voltage (V_{max}), and the maximum power point (MPP). The I-V stands for Current-Voltage and P-V curves are shaped by these parameters. The PV cell represented by a current source is connected parallel with a diode. The current, I_g , varies with the solar radiation level that the surface is exposed to. The current, I_d , which flows through the diode, is the main reason for the nonlinear I-V characteristic of the PV cell (**Figure 2**).

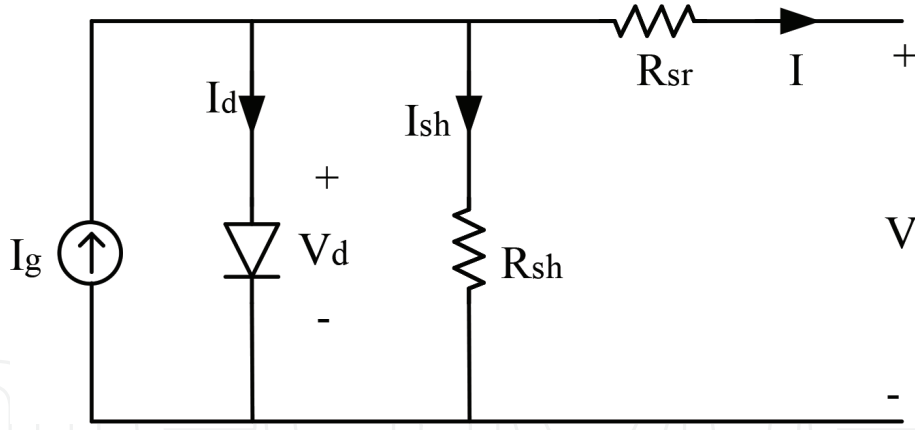


Figure 2.
Equivalent circuit of solar PV cell.

When we apply Kirchhoff's current law to the circuit,

$$I = I_g - I_d - I_{sh} \quad (1)$$

The substitution of the related expressions for the shunt branch current I_{sh} and diode current I_d in Eq. (1) yields the following:

$$I = I_g - I_0 \left[\exp \left(\frac{V + IR_{sr}}{\frac{nkT_c}{q}} \right) - 1 \right] - \left(\frac{V + IR_{sr}}{R_{sh}} \right) \quad (2)$$

I_g stands for the photocurrent, and it is the function of solar radiation on the cell and cell temperature:

$$I_g = I_{scR} \frac{G}{G_R} [1 + \alpha_T (T_c - T_{cR})] \quad (3)$$

The current I_0 in Eq. (2) is called the saturation current, a function of cell temperature, and given by

$$I_0 = I_{0R} \left(\frac{T_c}{T_{cR}} \right) \exp \left(\frac{1}{T_{cR}} - \frac{1}{T_c} \right) \frac{q e g}{n k} \quad (4)$$

A group of cells can be connected together either in a series or parallel combination. By connecting solar cells, PV modules can be created. Similarly, by connecting PV modules together, a PV array can be created. The output power of such PV systems can be calculated by the following equation:

$$P_{pv(t)} = H_t(t) x PVA x \mu_c(t) \quad (5)$$

$\mu_c(t)$ in Eq. (6) is the hourly efficiency of the PV system which can be obtained in terms of the cell temperature:

$$\mu_c(t) = \mu_{cr} [1 - \beta_t x (T_c(t) - T_{cr})] \quad (6)$$

$$T_c(t) = T_a + \lambda H(t) \quad (7)$$

$$PVA = \frac{1}{8760} \sum_{t=1}^{8760} \frac{P_{L,av}(t) F_s}{H_t \eta_c(t) V_f} \quad (8)$$

A PV panel generally consists of tempered glass, ethylene-vinyl acetate (EVA) layers, solar cells, and back-sheet materials shown in **Figure 3**. Tempered glass has been treated by heat or chemicals to increase its strength. Glass can be double or single due to increasing strength, but triple glass is not recommended because of reducing efficiency and low thermal transmittance. EVA is the adhesive material that includes ethylene, vinyl, and acetate chemicals, and its layers provide excellent thermal protection for solar cells. EVA layers provide to not pass too much of the sunshine trying to reach the solar cells. Back-sheet contributes to mechanical balance, durability for harsh weather, and high-performance properties for the PV module.

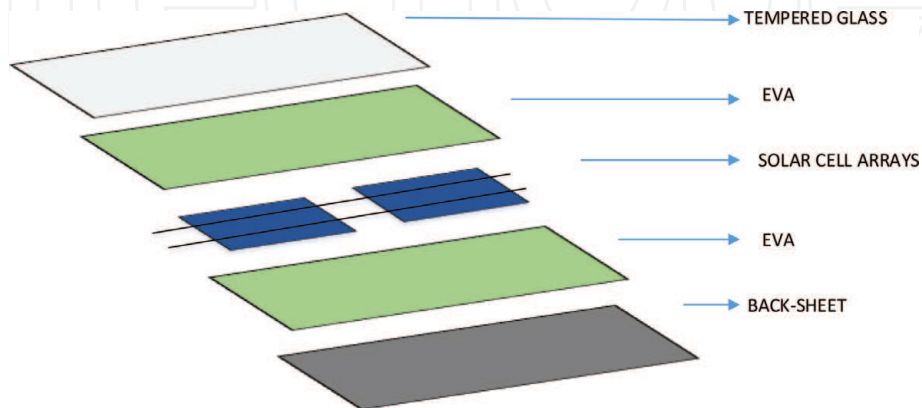


Figure 3.
 PV panel layout.

2.1.2 DC-DC boost converter

The input voltage of the step-up (boost) converter is always less than the output voltage. **Figure 4** shows the working principle of the DC-DC boost converter. **Figure 4(a)** shows the on state. This state is included to store power in the inductor, charge the inductor, which increases the current through the inductor.

Figure 4(b) shows the off state. This state is included to discharge power from the inductor into the load and the capacitor and decrease current through the inductor.

2.1.3 Three-phase inverter

Another component is the three-phase inverter shown in **Figure 5**. Inverters are generally used for high-power applications. A six-transistor and six-diode

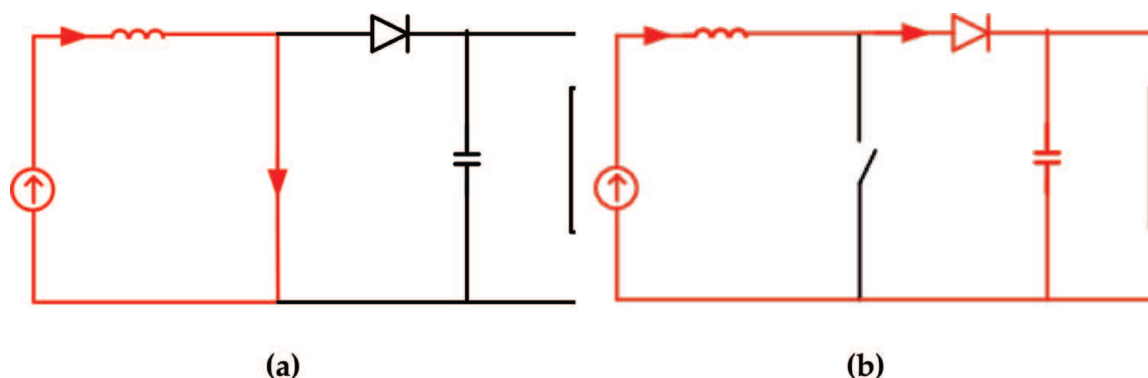


Figure 4.
 (a) On-state step-up converter and (b) off-state step-up converter.

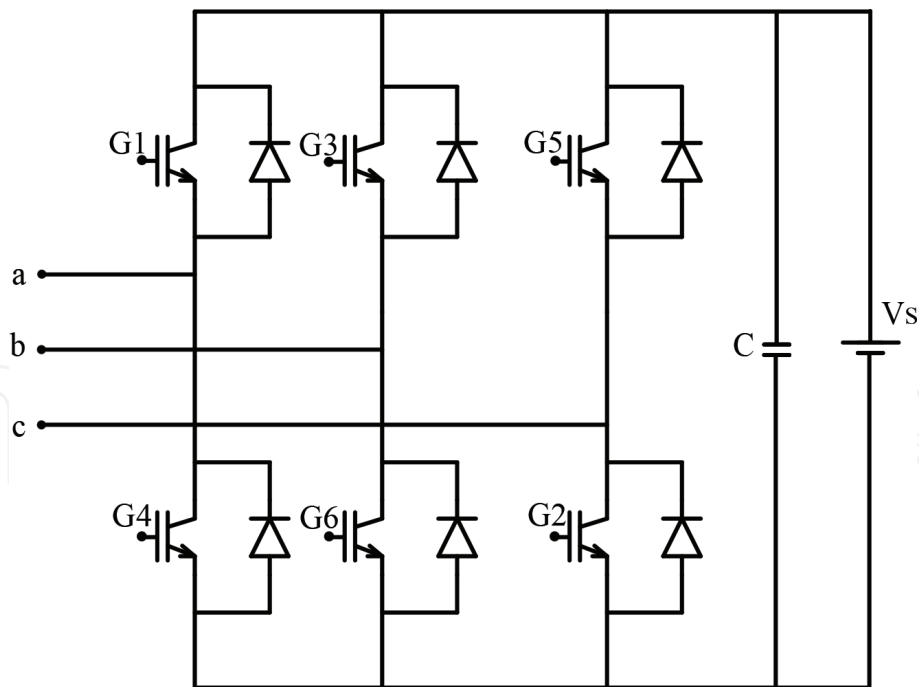


Figure 5.
Three-phase inverter.

Switch states for three-phase voltage source inverter					
State	State no	Switch states	V_{ab}	V_{bc}	V_{ca}
G5, G6, G1 on, others off	1	101	V_s	$-V_s$	0
G6, G1, G2 on, others off	2	100	V_s	0	$-V_s$
G1, G2, G3 on, others off	3	110	0	V_s	$-V_s$
G2, G3, G4 on, others off	4	010	$-V_s$	V_s	0
G3, G4, G5 on, others off	5	011	$-V_s$	0	V_s
G4, G5, G6 on, others off	6	001	0	$-V_s$	V_s
G1, G3, G5 on, others off	7	111	0	0	0
G2, G4, G6 on, others off	8	000	0	0	0

Table 1.
Switch states for three-phase voltage source inverter.

configuration is generally used for a three-phase output shown in the figure below. Two types of control signals can be applied to the transistors: 180° conduction and 120° conduction. The 180° conduction provides for better usage of the switches and is the preferred method. The switch states for a three-phase voltage source inverter (VSI) are shown in **Table 1**.

2.2 Wind system

2.2.1 Wind turbine

Wind turbine technology is developed day by day, and several models are designed to increase the power capability of the wind turbines. The mechanical power of the wind turbine is related to its power coefficient C_p and wind velocity v and represented by

$$P_{mech} = \frac{1}{2} C_p \rho \pi R^2 v^3 \quad (9)$$

The air density is represented by ρ , and the radius of the turbine propeller, given by Eq. (9), is represented by R . The power coefficient can be described as the ratio of the electric power produced by a wind turbine divided by the total amount of wind power flowing into the turbine blades at a certain wind speed. Every wind turbine has a unique power coefficient value. Power coefficient is broadly defined as a function of the tip/speed/ratio λ , and the equation is given by the value w corresponding to the rotational speed of the wind turbine:

$$\lambda = \frac{wR}{v} \quad (10)$$

When λ gets a specific value, it ensures a maximum of C_p . Turbine rotational speed value provides to capture the maximum mechanical power attainable from the wind for a specific wind velocity. Thus, turbine speed is followed precisely. When the power coefficient is assumed to be at the optimum for a particular wind turbine, the tip/speed/ratio values producing the maximum mechanical power of the wind turbine reach their optimum value. This operation is effective only if the nominal wind speed with the existing wind power does not exceed the rated capacity of the generator.

2.2.2 Doubly fed induction generator

The back-to-back converter is a bidirectional frequency converter. This means that it must manage power flow in both directions. The RSC and GSC and a common DC bus combine to form this back-to-back converter. Park's model is a special model frequently used for induction generators. The study analysis is easier when the rotor variables are referred to the stator side. A rotating reference frame is more preferable, but in this study, a static stator-oriented reference frame is more appropriate. Also, linear magnetic circuits are not negligible. Park's model can be expressed by the equations below:

$$v_s = R_s i_s + \frac{d}{dt} \phi_s \quad (11)$$

$$v_r = R_r i_r + \frac{d}{dt} \phi_r - jw\phi_r \quad (12)$$

For this model, v is the voltage, i is the current, R is the resistance, ϕ is the magnetic flux, and w is the rotor electrical speed. The subscripts s and r indicate stator and rotor quantities.

Stator voltage depends on the grid because of the connection of the stator to the grid. The machine is controlled by the rotor voltage v_r because rotor voltage is adjusted by the converter. The stator and rotor fluxes are given by

$$\phi_s = L_s i_s + L_m i_r \quad (13)$$

$$\phi_r = L_r i_r + L_m i_s \quad (14)$$

L_s and L_r are expressed as the stator and rotor inductance. L_m is the magnetizing inductance. Rotor voltage is the relatively important variable. This voltage can be calculated from Eqs. (15) and (16):

$$v_{r0} = \frac{L_m}{L_s} \left(\frac{d}{dt} - j\omega \right) \phi_s, \sigma = 1 - \frac{L_m^2}{L_s L_r} \quad (15)$$

where σ is the leakage factor and σL_r is the rotor transient inductance. Eqs. (12) and (15) yield

$$v_r = \frac{L_m}{L_s} \left(\frac{d}{dt} - j\omega \right) \phi_s + \left(R_r + \sigma L_r \left(\frac{d}{dt} - j\omega \right) \right) i_r \quad (16)$$

v_r is the rotor voltage presented in Eq. (16). If the rotor is an open-circuit state, it means that i_r is equal to 0 and one term of the rotor voltage is v_{r0} given by Eq. (17).

$$v_{r0} = \frac{L_m}{L_s} \left(\frac{d}{dt} - j\omega \right) \phi_s \quad (17)$$

Another term of the rotor voltage (v_r) exists when the current (i_r) flows in the rotor. Voltage drop existing on rotor resistance (R_r) and the rotor transient inductance (σL_r) cause rotor voltage.

2.2.3 Rotor-side and grid-side converters

The main task of the RSC is to manage the reactive power and the active power of the generator. The fluctuations that affect stator reactive power and the electromagnetic torque are also removed by the RSC. The main task of the GSC is to maintain DC-link voltage stability against all possible directions and magnitudes of the rotor power. In addition, the GSC is responsible to ensure operation with zero reactive power, in other words, with a unity power factor. That is to say, the GSC does not exchange reactive power; it only exchanges active power with the grid. As a result, it can be said that the reactive power exchange is only carried out by the stator.

3. Control of the proposed system

The circuit topology and the controller of the proposed system can be seen in **Figure 6**. There are two main parts to the controller of the proposed system: the PV system and wind system controllers.

3.1 Maximum power point tracking (MPPT)

The terminal voltage of the photovoltaic system is generally adjusted according to the MPP voltage by an incremental conductance method. MPP is obtained from the instantaneous conductance of the photovoltaic module in comparison to the incremental conductance of the solar photovoltaic module. While instantaneous conductance is the current divided by the voltage, incremental conductance is the difference in current divided by the difference in voltage:

$$\frac{\Delta I}{\Delta V} = \frac{I}{V} \quad (18)$$

$$\frac{\Delta I}{\Delta V} > -\frac{I}{V} \quad (19)$$

$$\frac{\Delta I}{\Delta V} < -\frac{I}{V} \quad (20)$$

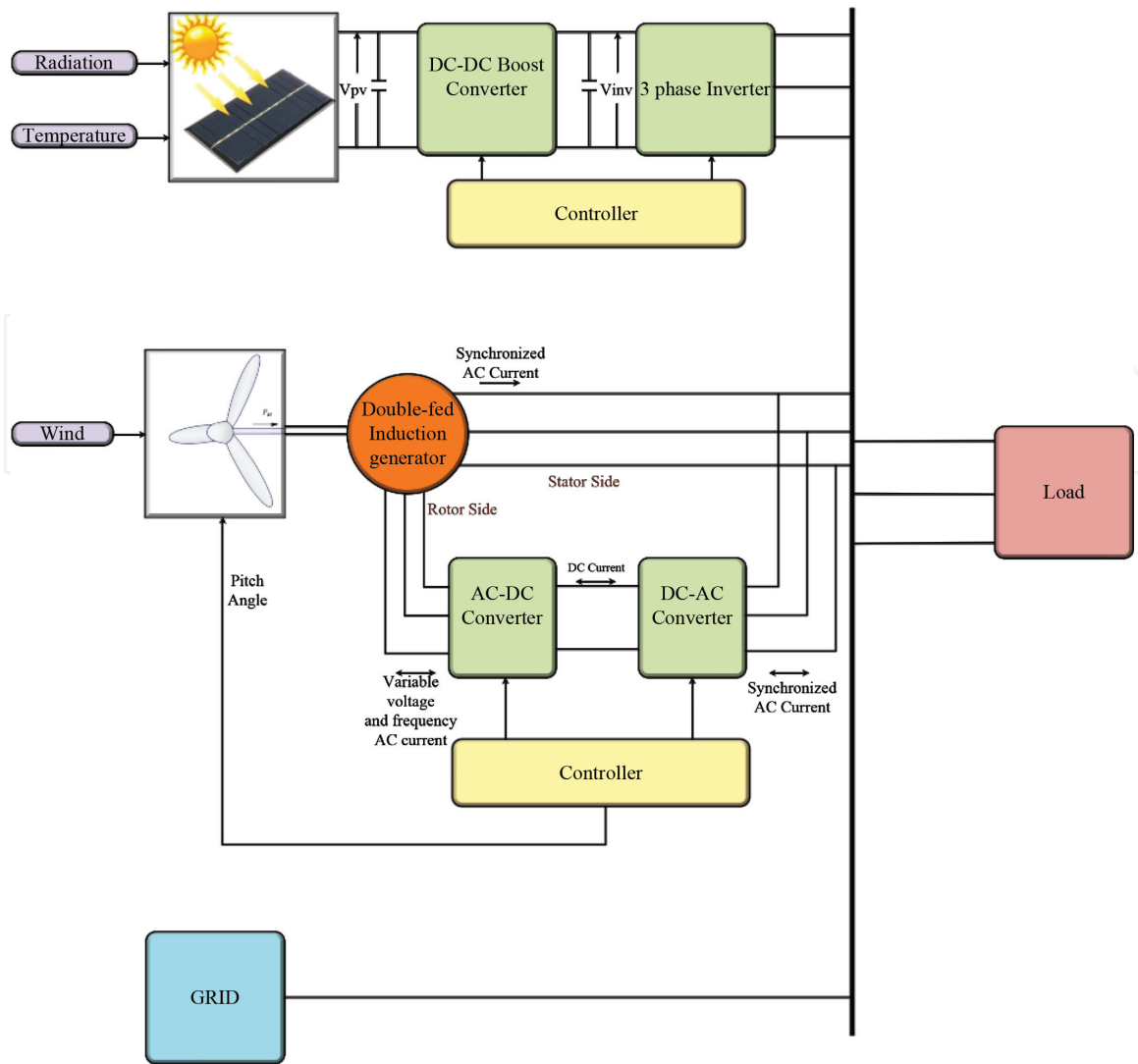


Figure 6.
 Proposed system and controller.

Eq. (18) shows that the PV module is operating at the MPP. Equation (19) shows the left-hand region of the MPP on the P-V curve, and Eq. (20) shows the right-hand region of the MPP on the P-V curve. The slope of the P-V curve is equal to zero at MPP and is given by Eq. (21):

$$\frac{dP}{dV} = 0 \quad (21)$$

And also

$$\frac{dP}{dV} = I \left(\frac{dV}{dV} \right) + V \left(\frac{dI}{dV} \right) \quad (22)$$

$$\frac{dP}{dV} = I + V \left(\frac{dI}{dV} \right) \quad (23)$$

By using Eq. (21) and Eq. (23), Eq. (24) is derived and it has small permitted errors

$$\left| I + V \left(\frac{dI}{dV} \right) \right| = e \quad (24)$$

The incremental method is used to find the MPP of the PV module. It helps to reduce power loss and system cost and improve the PV efficiency. It has the great

advantage of being a fast power tracking process. However, if the solar irradiation is low due to a small current differentiation, it will be unbalanced, but it has more accuracy, higher efficiency, and a faster power tracking process than other methods. The detailed block diagram and controller are shown in **Figures 7 and 8**.

3.2 DC-DC boost converter controller

There are different types of controllers for different industries. Proportional-integral (PI) controllers are appropriate for various application areas. By tuning the parameters of these controllers, the desired output can be produced. This is a primary necessity in the implementation of these controllers. For this reason, the adjustment of the parameters of the controller has to be done with high speed and high accuracy shown in **Figure 9**.

3.3 Three-phase inverter controller

The difference between the measured DC-link value of the inverter and the reference DC-link voltage was calculated. The error signal obtained by the conventional PI controller was used for the comparison of reference PI signals with carrier signals to generate the gate signals shown in **Figure 10**.

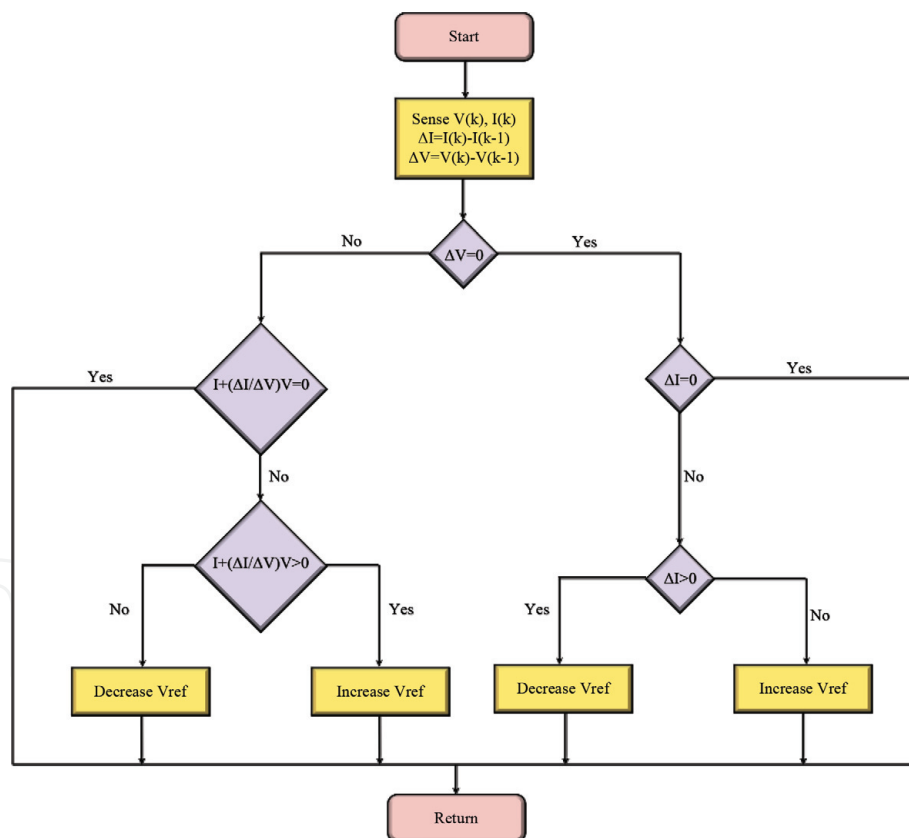


Figure 7.
Incremental method block diagram.

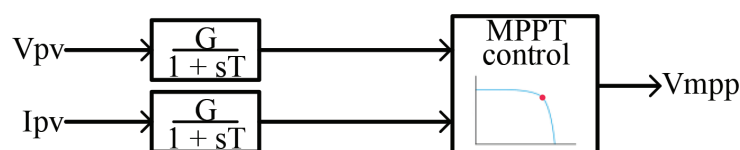


Figure 8.
MPPT controller.

3.4 Wind system controller

DFIG is named as “doubly fed” because two electrical parts of the machine called as stator and rotor are connected to electrical sources, as shown in **Figure 11**. There is a direct connection between the electric grid and the stator circuit; however, rotor windings are linked to an AC/DC/AC converter over slip rings. The converter consists of two types of converters: the RSC (C_{rotor}) and the GSC (C_{grid}). In **Figure 11**, the capacitor performs as the DC voltage source. A coupling inductor, L , exists between the GSC and the grid used to connect to C_{grid} . The induction generator converts the rotational power of the wind turbine into electrical power and this generated power is transferred to the electrical grid. In addition, pitch angle commands are used to regulate the generated power of the wind turbine, the DC busbar voltage, and also the reactive power—or the voltage at the grid terminals. Pitch angle control is also enabled to limit the maximum output power to protect the generator against a blast of wind.

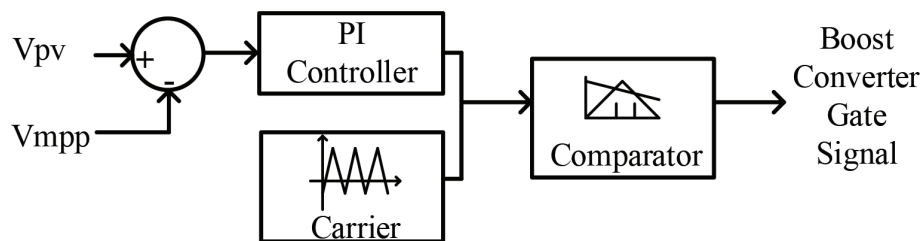


Figure 9.
 DC-DC boost converter controller.

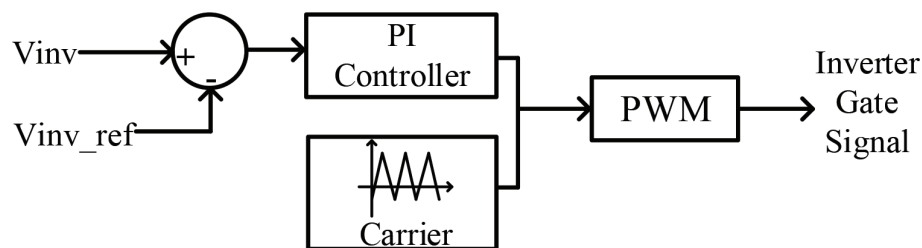


Figure 10.
 Three-phase inverter controller.

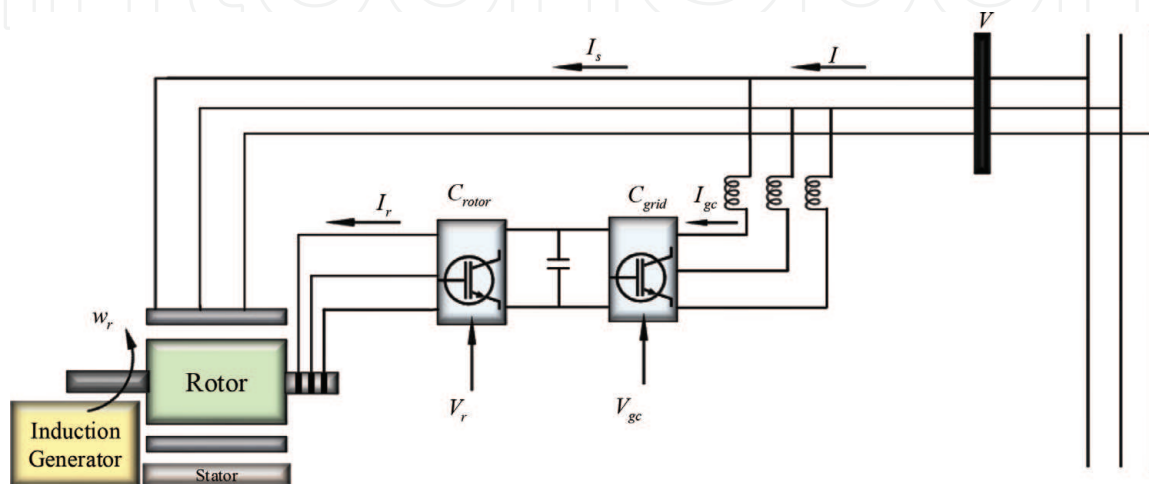


Figure 11.
 DFIG-based wind system.

The torque and speed of the DFIG shown in **Figure 11** are controlled by the RSC. The RSC primarily aims to control the rotor currents and thus deliver the desired torque at the shaft of the machine. The RSC regulates the output power of the wind turbine thanks to the torque controller. The real generated power appearing at the grid side of the wind turbine is added to both the mechanical and electrical power losses and is compared to the reference power. The rotor speed error is reduced by using a proportional-integral controller. The reference rotor current added in the rotor windings by the RSC controls the electromagnetic torque T_e . The actual I_{qr} component of the positive sequence current is compared to I_{qr_ref} , and the error is minimized to zero by using a proportional-integral controller. The output of the controller for regulating the current is the voltage V_{qr} generated by C_{rotor} (**Figure 12**).

The GSC provides the flowing control of the real and reactive power from the turbine system to the grid, as shown in **Figure 13**. DC bus capacitor voltage is regulated by the grid-side converter. The control system consists of two control loops. A DC voltage controller forms the outer regulation loop. The current controller uses the output of the DC voltage controller as the reference current. A current controller and feed-forward terms which predict C_{grid} —the output voltage—form the inner regulation loop. This loop regulates the magnitude and phase of the GSC-generated voltage (V_{gc}) from the I_{dgc_ref} generated by the DC voltage controller and indicated by I_{q_ref} reference.

Pitch angle control is necessary to protect against network faults shown in **Figure 14**. When the network experiences a fault, the generator continues to generate power; therefore the DC-link capacitance will be overcharged. This means

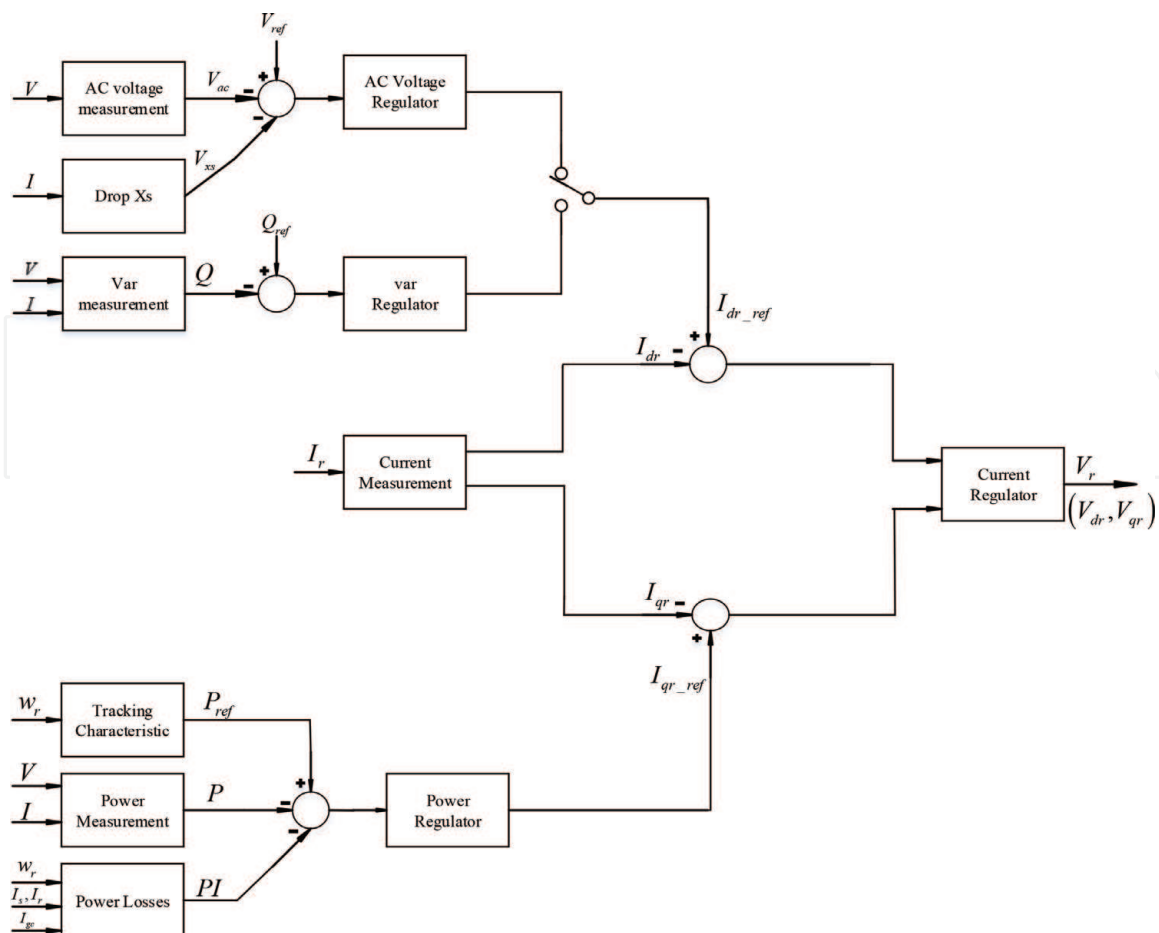


Figure 12.
 RSC controller.

that there is no control over the blade speed and the torque. Pitch angle control is often preferred to braking mechanisms.

In addition to these measures, the reactive current flowing in the RSC controls the reactive power at the grid terminals. The wind turbine has two regulation

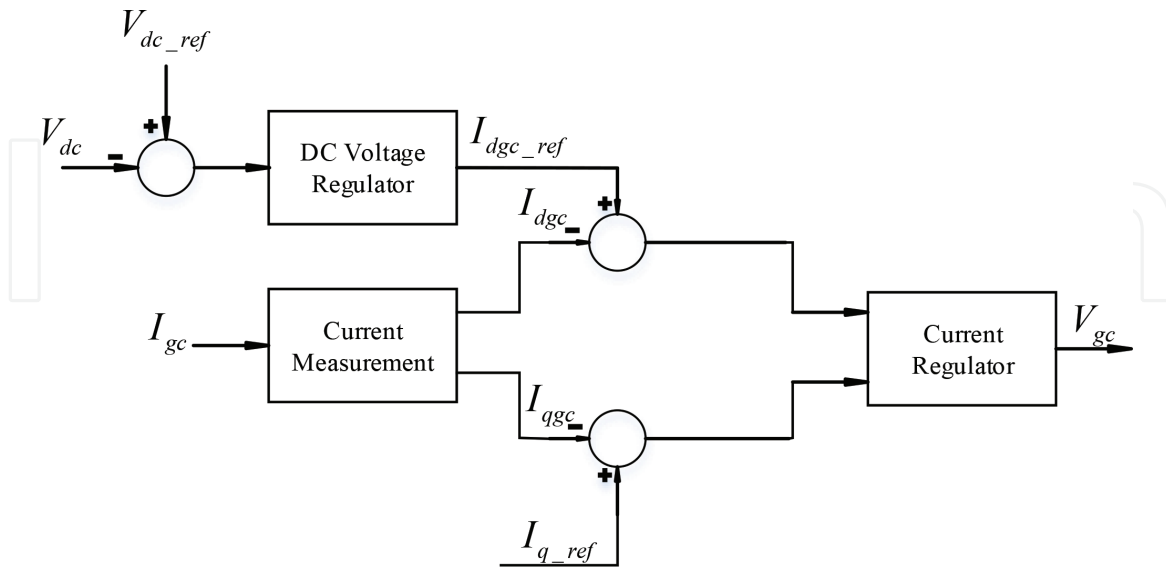


Figure 13.
GSC controller.

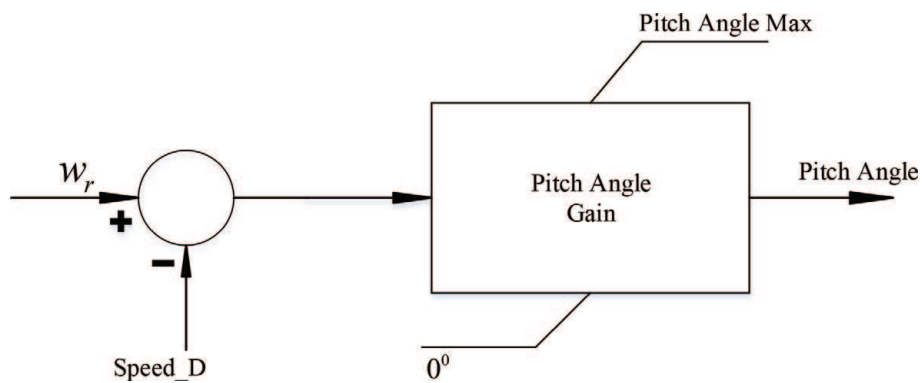


Figure 14.
Pitch angle controller.

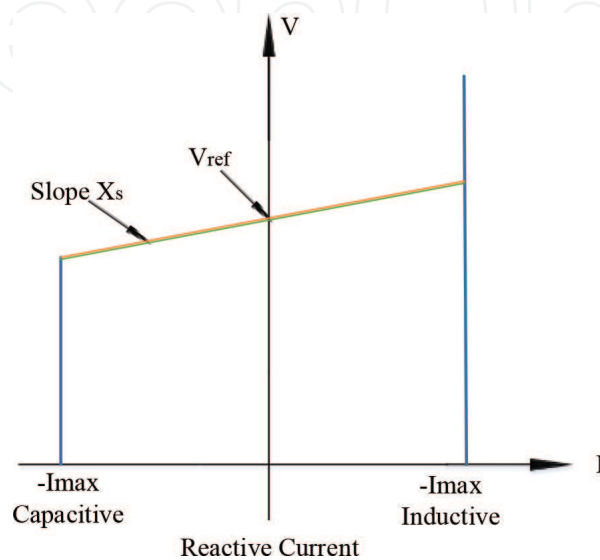


Figure 15.
I-V characteristic curve.

modes. The first of these is the voltage regulation mode; it fulfills the following I-V characteristic shown in **Figure 15**.

When the reactive current reaches the maximum current values, the voltage is optimized by the reference voltage V_{ref} , and the I-V characteristic has a specified slope shown in **Figure 15**. Another mode is the VAR regulation mode; the VAR controller provides constant reactive power at the grid terminals.

As a result, doubly fed induction generators are components that generate electricity in wind turbines. While the power generated by the wind turbine is converted into electrical power, they adjust the amplitude and frequency of their output voltages to maintain them at a constant value and also control the power factor thanks to their control mechanism and structure.

4. Results and discussion

The combined PV/wind system with real dynamic input datasets was validated by a simulation program called PSCAD/EMTDC. The simulation aims to evaluate the accuracy and efficacy of the control strategy used for implementation in power distribution systems. The related parameters of the proposed system are shown in **Table 2**. The nominal frequency of the power grid is 50 Hz for this simulation.

In this chapter, the configuration includes a variable speed-controlled wind turbine and a DFIG. This topology is used for tracking the efficient use of wind

Parameters	Value
480 kW PV array	
Series-connected PV modules	20
Parallel-connected PV modules	16
Series-connected PV cells	108
Parallel-connected PV cell strings	12
Reference solar radiation	1000 W/m ²
Reference PV panel temperature	25°C
PV cell	
Effective area	0.01 m ²
Series resistance	0.02 ohm
Shunt resistance	1000 ohm
Ideality factor of the diode	1.5
Bandgap energy	1.103 eV
Saturation current	10 ⁻⁹ A
Short circuit current	2.5 A
Wind energy conversion system	
Cut-in speed	4 m/s
Rated speed	10.5 m/s
Cut-out speed	25 m/s
Rated power	5.1 MVA

Table 2.
Parameters of proposed system.

power. The power coefficient, C_p , which is a function of wind speed/machine speed is selected to be 1.2 p.u. (per unit). For this reason, the variations in wind speed require variation in machine speed in order to keep the system operating at maximum C_p . In the C_p implementation used here, the nominal power of the turbine is obtained when rotating at 1.2 p.u. mechanical speed. As described earlier, RSC and GSC were used in this topology. The GSC is in charge of controlling the DC-link voltage, and the reactive power control is normally set to inject zero Q (reactive power of the system) for this converter.

As seen from **Figure 16**, the cut-in speed is 4 m/s. The turbine has an oscillation in its power rate and voltage level after start-up. It can be because of the synchronization point with the grid. A start-up PI controller is used to set up the voltage on the stator terminals before synchronizing. The rated speed is 11 m/s. Beyond the rated speed, output power is almost constant even if the wind speed accelerates. As the wind speed increases above the rated speed, the mechanical force on the wind turbine increases. After a certain point, this force may damage the turbine. Because

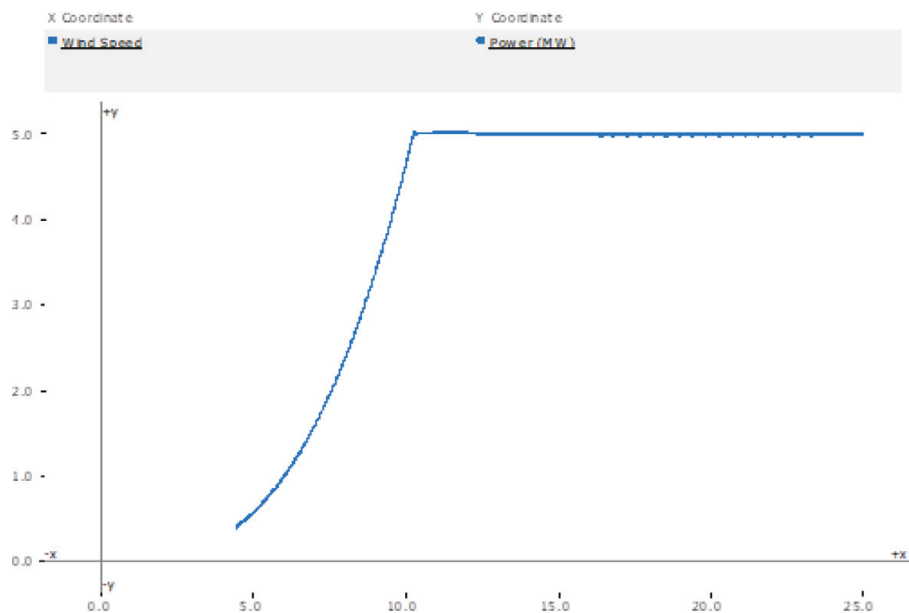


Figure 16.
 The curve of wind speed versus output power.

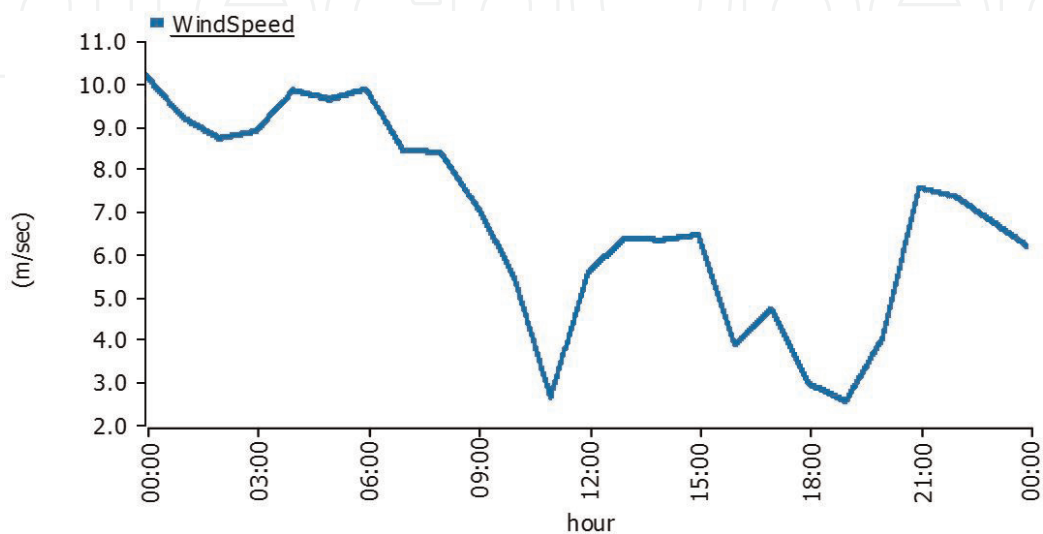


Figure 17.
 Wind speed versus hour for 1 day.

of this, the braking system to stop the rotor beyond a certain wind speed—which is called the cut-out speed—is reached. The cut-out speed is almost 25m/s.

The data included in **Figure 17** includes wind speed in units of m/sec over a 24-hour period.

The solar irradiance in units of W/m^2 is represented by a 24-hour time scale in **Figure 18**. As shown above, the solar power varies over the day, and it has its peak value at noon. This is the cell temperature (in units of degrees centigrade) graphic in **Figure 18**, which is also important for power generation from the solar energy source.

This is the cell temperature in units of centigrade degree ($^{\circ}C$) graphic in **Figure 18** which is also important for the power generation from the solar energy source.

The active power flow seen from the point of common coupling (PCC) during a day is shown in **Figure 19**. **Figures 18–20** show that PV plant generates power only when solar radiation is available (in this case between 6 a.m. and 4 p.m.), and the output of wind power generation system is proportional to wind speed. The graph of the load which is real consumption data of a neighborhood and the graph of active power flow to the electrical grid are also seen at **Figure 19**. When the electric power demand of the loads is greater than the total produced power by wind power generation system and the PV power generation system, the lacking power is

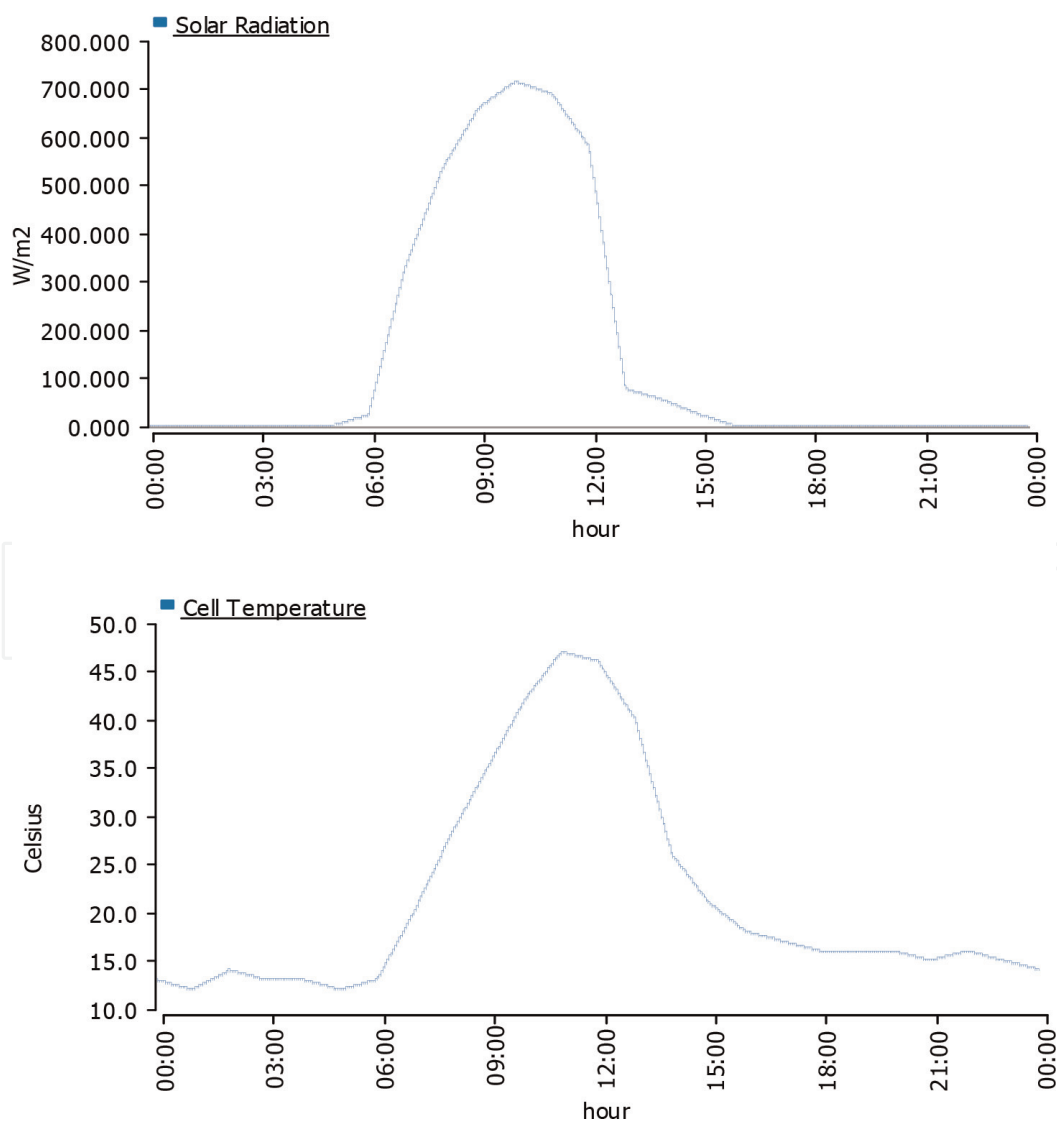


Figure 18.
Solar radiation and cell temperature versus hour for 1 day.

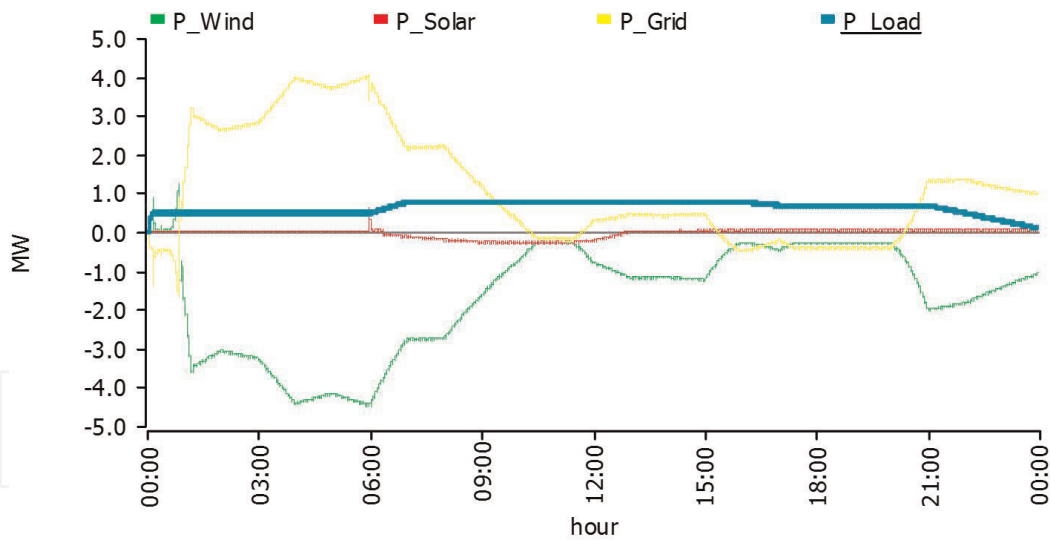


Figure 19.
Active power flow versus hour for 1 day.

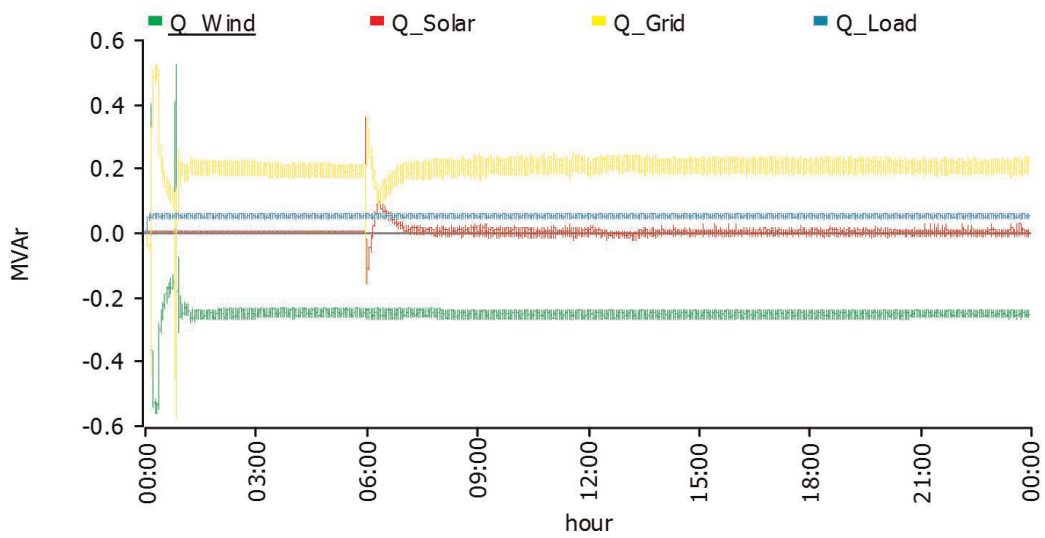


Figure 20.
Reactive power flow versus hour for 1 day.

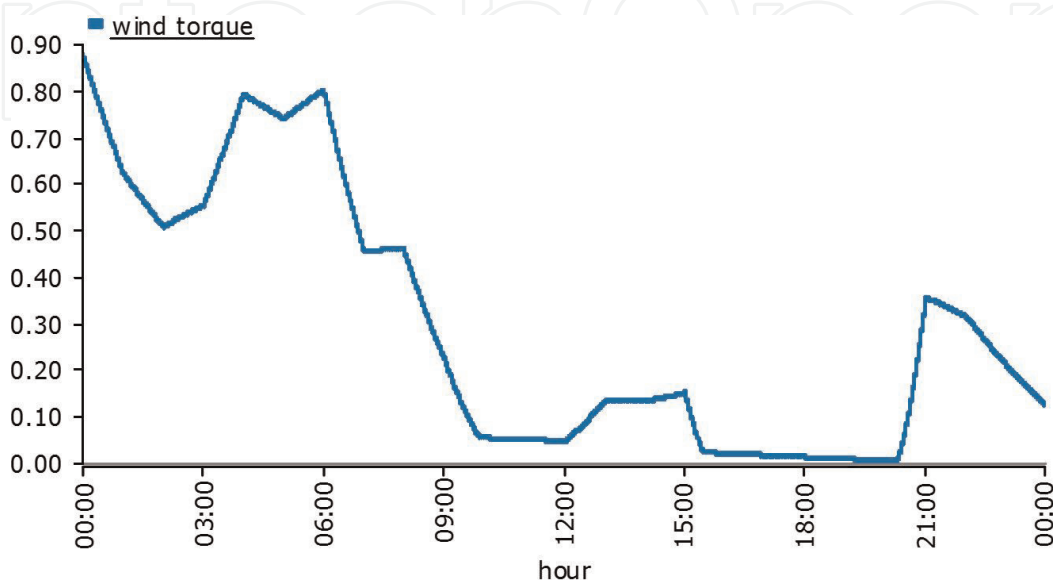


Figure 21.
Wind torque versus hour for 1 day.

provided from the electrical grid. Contrary, when the power demand of the loads is less than the total produced power by wind power generation system and PV power generation system, the remaining power is transferred to the electrical grid.

The reactive power flow seen from the PCC is shown in **Figure 20**. It is wind torque graphic in **Figure 21** which changes according to wind speed.

5. Conclusion

In this chapter, attention is mainly focused on the power control of a combined PV/wind system for power generation. The goal is to use real data from both the combined PV/wind systems and observe the system reliability with real-time simulation results. In this simulated PV/wind system, it is engineered to reach the maximum energy available from real conditions of wind speed and solar irradiance using dynamic input datasets. The simulation results illustrate and verify the operation and control of the proposed system. The chapter showed that the use of renewable energy resources provides higher energy potential, cost efficiency, operating and maintenance costs, an effective solution to energy demand, an attractive investment alternative, and environmental sustainability. Moreover, the period of financial return is shortened thanks to a combined PV/wind system, compared to stand-alone PV or wind systems. In addition, the sun and wind energy complete each other when the weather conditions are continuously changing. Thereby, energy production is provided all the time, and the system reliability is also consolidated by preventing sudden electrical loss. This chapter is a great example for further studies in terms of applicability because a real PV/wind system can be established, observed, and supported by performing simulation studies.

Author details

Emel Bakmaz¹, Kemal Aygul¹, Burak Esenboga², Tugce Demirdelen^{2*} and Mehmet Tumay²

¹ Department of Electrical and Electronics Engineering, Cukurova University, Adana, Turkey

² Department of Electrical and Electronics Engineering, Adana Alparslan Turkes Science and Technology University, Adana, Turkey

*Address all correspondence to: tdemirdelen@atu.edu.tr

IntechOpen

© 2020 The Author(s). Licensee IntechOpen. Distributed under the terms of the Creative Commons Attribution - NonCommercial 4.0 License (<https://creativecommons.org/licenses/by-nc/4.0/>), which permits use, distribution and reproduction for non-commercial purposes, provided the original is properly cited. 

References

- [1] González A, Riba J-R, Rius A. Optimal sizing of a hybrid grid-connected photovoltaic-wind-biomass power system. *Sustainability*. 2015;7:12787-12806
- [2] Jain S, Karampuri R, Somasekhar VT. An integrated control algorithm for a single-stage PV pumping system using an open-end winding induction motor. *IEEE Transactions on Industrial Electronics*. 2016;63:956-965
- [3] Long H, Eghlimi M, Zhang Z. Configuration optimization and analysis of a large scale PV/wind system. *IEEE Transactions on Sustainable Energy*. 2017;8:84-93
- [4] Patra S, Ray PK, Mohanty A. Robust fuzzy-sliding mode based UPFC controller for transient stability analysis in autonomous wind-diesel-PV hybrid system. *IET Generation Transmission and Distribution*. 2016;10:1248-1257
- [5] Parida A, Chatterjee D. Model-based loss minimisation scheme for wind solar hybrid generation system using (grid-connected) doubly fed induction generator. *IET Electric Power Applications*. 2016;10:548-559
- [6] Al-Masri HM, Ehsani M. Feasibility investigation of a hybrid on-grid wind photovoltaic retrofitting system. *IEEE Transactions on Industry Applications*. 2016;52:1979-1988
- [7] Shen C-L, Shen Y-S. Output filter design for a novel dual-input PV-wind power converter by energy balance principle. *Applied Sciences*. 2016;6:263
- [8] Cho J-H, Chun M-G, Hong W-P. Structure optimization of stand-alone renewable power systems based on multi object function. *Energies*. 2016;9:649
- [9] Kalla UK, Singh B, Murthy SS, Jain C, Kant K. Adaptive sliding mode control of standalone single-phase microgrid using hydro, wind, and solar PV array-based generation. *IEEE Transactions on Smart Grid*. 2018;9:6806-6814
- [10] Palmer D, Koubli E, Cole I, Betts T, Gottschalg R. Comparison of solar radiation and PV generation variability: System dispersion in the UK. *IET Renewable Power Generation*. 2017;11:550-557
- [11] Ekstrom J, Koivisto M, Mellin I, Millar RJ, Lehtonen M. A statistical model for hourly large-scale wind and photovoltaic generation in new locations. *IEEE Transactions on Sustainable Energy*. 2017;8:1383-1393
- [12] Liu Y, Tan S, Jiang C. Interval optimal scheduling of hydro-PV-wind hybrid system considering firm generation coordination. *IET Renewable Power Generation*. 2017;11:63-72
- [13] Luna AC, Diaz NL, Graells M, Vasquez JC, Guerrero JM. Mixed-integer-linear-programming-based energy management system for hybrid pv-wind-battery microgrids: Modeling, design, and experimental verification. *IEEE Transactions on Power Electronics*. 2017;32:2769-2783
- [14] Shanthi P, Uma G, Keerthana MS. Effective power transfer scheme for a grid connected hybrid wind/photovoltaic system. *IET Renewable Power Generation*. 2017;11:1005-1017
- [15] Merabet A, Tawfique Ahmed K, Ibrahim H, Beguenane R, Ghias AMYM. Energy management and control system for laboratory scale microgrid based wind-PV-battery. *IEEE Transactions on Sustainable Energy*. 2017;8:145-154
- [16] Basaran K, Cetin NS, Borekci S. Energy management for on-grid and

off-grid wind/PV and battery hybrid systems. *IET Renewable Power Generation*. 2017;**11**:642-649

[17] Askarzadeh A. Electrical power generation by an optimised autonomous PV/wind/tidal/battery system. *IET Renewable Power Generation*. 2017;**11**: 152-164

[18] Kant K, Jain C, Singh B. A hybrid diesel-wind PV-based energy generation system with brushless generators. *IEEE Transactions on Industrial Informatics*. 2017;**13**:1714-1722

[19] Rezkallah M, Hamadi A, Chandra A, Singh B. Design and Implementation of active power control with improved P&O method for wind-PV-battery-based standalone generation system. *IEEE Transactions on Industrial Electronics*. 2018;**65**:5590-5600

[20] Tiwari SK, Singh B, Goel PK. Design and control of autonomous wind-solar system with DFIG feeding 3-phase 4-wire loads. *IEEE Transactions on Industry Applications*. 2018;**54**: 1119-1127

[21] Einan M, Torkaman H, Pourgholi M. Optimized fuzzy-cuckoo controller for active power control of battery energy storage system, photovoltaic, fuel cell and wind turbine in an isolated micro-grid. *Batteries*. 2017;**3**:23

[22] Ji H, Niu D, Wu M, Yao D. Comprehensive benefit evaluation of the wind-PV-ES and transmission hybrid power system consideration of system functionality and proportionality. *Sustainability*. 2017; **9**:65

[23] Mendoza-Vizcaino J, Sumper A, Galceran-Arellano SPV. Wind and storage integration on small islands for the fulfilment of the 50-50 renewable electricity generation target. *Sustainability*. 2017;**9**:905

[24] Liu Y, You S, Liu Y. Study of wind and PV frequency control in U.S. power grids—EI and TI case studies. *IEEE Power and Energy Technology Systems Journal*. 2017;**4**:65-73

[25] Hussain S, Al-ammari R, Iqbal A, Jafar M, Padmanaban S. Optimisation of hybrid renewable energy system using iterative filter selection approach. *IET Renewable Power Generation*. 2017;**11**: 1440-1445

[26] Akram U, Khalid M, Shafiq S. An innovative hybrid wind-solar and battery-supercapacitor microgrid system—Development and optimization. *IEEE Access*. 2017;**5**: 25897-25912

[27] Akram U, Khalid M, Shafiq S. Optimal sizing of a wind/solar/battery hybrid grid-connected microgrid system. *IET Renewable Power Generation*. 2018;**12**:72-80

[28] Gonzales Arispe JC, Ponce Vasquez AB. Wind and PV farms integration within power systems using static and dynamic simulations. *IEEE Latin America Transactions*. 2018;**16**:148-154

[29] Khaled U, Eltamaly AM, Beroual A. Optimal power flow using particle swarm optimization of renewable hybrid distributed generation. *Energies*. 2017;**10**:1013